Phase diagram for a generalized fully frustrated triangular XY model

G. Parker and W. M. Saslow
Center for Theoretical Physics, Department of Physics, Texas A&M University, College Station, Texas 77843-4242

M. Gabay
Center for Theoretical Physics, Department of Physics, Texas A&M University, College Station, Texas 77843-4242 and Laboratoire de Physique des Solides, Université de Paris–Sud, 91405 Orsay, France

(Received 19 April 1990; revised manuscript received 20 December 1990)

To better understand the phase diagram for XY spins on the fully frustrated triangular lattice, we generalize that model, giving one class of bonds a "tunable" strength $-\eta J$, where $\eta=1$ gives the conventional model. As a consequence, the sites are no longer all equivalent. Using mean-field theory, the phase diagram has been determined as a function of η, the applied field H, and the temperature T. For $H=0$, the phase diagram is very similar to that for the generalization of Berge *et al.* of the fully frustrated XY square lattice model. For $H\neq 0$ and $-0.5<\eta<1.$, a nonuniform collinear phase intervenes between two noncollinear phases (one chiral and the other nonchiral). This nonuniform collinear phase is an extension of the paramagnetic phase (which, in a field, also is nonuniform and collinear), rather than being the (spontaneous symmetry-breaking) nonuniform collinear Potts phase of the $\eta=1$ Monte Carlo phase diagram. For $\eta<-0.5$ this extension of the paramagnetic phase completely displaces the (low-field) chiral phase. For $\eta>1$ the extension of the paramagnetic phase is absent. For $\eta=1$ we conclude that the simplest explanation for the Potts phase can be obtained by comparison to the Monte Carlo phase diagram for Ising spins on this lattice.

I. INTRODUCTION

Spin glasses[1] are characterized by both randomness and frustration. To separate their effects, it has proven useful to study systems that are periodic but fully frustrated, meaning that no plaquette of Ising spins is "satisfied" in the ground state. With XY spins the test of frustration is the same as for Ising spins ($\prod_i J_{ij}<0$, taken around a plaquette), but the frustrated ground state is characterized by canting or spin tipping. Examples of fully frustrated models are the Villain model[2] on square and cubic lattices[3] and the antiferromagnetic (AF) fully frustrated triangular lattice (FFTR).[4]

In the present paper we introduce a generalization of the FFTR, in which one of the antiferromagnetic bonds $-J$ is replaced by a bond of strength $-\eta J$, using mean-field theory to look at the phase diagram in the magnetic field (H) and temperature (T) plane. In this model, unlike the FFTR, the sites are not all equivalent.

Our motivation for this study was threefold. (1) The $\eta=1$ Monte Carlo results of Refs. 5 and 6 yield at finite H a "Potts-like" phase that does not appear in mean field theory,[7] and so it was felt that study of a generalized version of the FFTR model would shed light on the origin of the Potts like phase. Note that in zero field the temperature at which ordering begins is about a factor of 3 lower in the Monte Carlo than in the mean-field calculations because of the effect of fluctuations.[5–7] (2) A non-fully-frustrated generalization of the fully frustrated Villain model has been studied in Monte Carlo,[8] yielding results that can be interpreted using the energy scales associated with mean-field theory.[9] This generalization has clarified the behavior of the system for $H=0$, where, on crossing from the paramagnetic phase to the ordered phase, continuous (XY) and discrete (helicity or Ising) types of order develop simultaneously.[5,6,10] (3) It is possible to map from the problem of coupled XY spins to the problem of coupled Josephson junctions, by taking a suitable choice of electromagnetic gauge,[11] and by suitable lithography, one can in principle actually produce arrays of superconducting islands coupled by such Josephson junctions.

Work on fully frustrated systems indicates that when such a system orders, it simultaneously develops both XY and Ising types of order. By breaking some of the degeneracy in the problem, it is possible to separate the transitions and to gain insight about the physical mechanisms associated with each type of order. Much effort in this direction has been expended in trying to determine a correct physical picture for the transitions.[12] As was the case for the Berge *et al.* generalization of the Villain model on the square lattice,[8] a consistent picture of the transitions can be provided by considering the mean-field energy scales associated with competing collinear ordering, and the requirement that order be defined locally before it can be destroyed by the topological excitations associated with a Kosterlitz-Thouless transition.

An outline of the paper is as follows. In Sec. II we define our generalized version of the FFTR model and summarize the results of mean-field theory for $\eta=1$. In Sec. III we discuss the (new) method of iteration contrast plots (IC plots), which we found useful in our initial exploration of the solutions to the mean-field equations for

$\eta \neq 1$, where we did not initially know the nature of the phase diagram. In Sec. IV we study the mean-field phase diagram for $\eta < 1$. This is done in two stages. First, in H-T space, we study the convergence properties of the mean-field equations using IC plots. This leads to an identification of the interesting parts of the H-T plane. With this knowledge the mean-field equations are then solved to obtain the phase boundaries. In Sec. V we study the phase diagram for $\eta > 1$, a case that is simpler than for $\eta < 1$, although the IC plots shows that for a large region of the H-T plane the mean-field equations converge relatively slowly. In Sec. VI we describe the phase diagram in the η-T plane for $H=0$. The $H=0$ phase diagrams for the present model and for the generalization Villain model of Berge *et al.* are then compared. Section VII contains our concluding remarks, including the mean-field energy scale arguments that give a consistent picture of the order of the phase transitions, and presents a discussion of various works that shed light on the Potts phase that appears for $\eta=1$ and $H\neq 0$.[6]

II. GENERALIZED FULLY FRUSTRATED TRIANGULAR (FFTR) MODEL

In analogy to the generalization by Berge *et al.* of Villain's fully frustrated model of XY spins on a square lattice,[2,8] we want to generalize the fully frustrated model of XY spins on a triangular lattice[4] (FFTR). Our generalization is shown in Fig. 1. Every third horizontal bond is given a bond strength of $-\eta J$ instead of $-J$, as in the pure AF case. In Fig. 1 the $-\eta J$ bonds ($\frac{1}{9}$ of the total number) are represented as double lines and the $-J$ bonds as single lines ($\frac{8}{9}$ of total). One-third of the sites have six $-J$ bonds, and two-thirds of the sites have one $-J$ and five $-\eta J$ bonds. This leads to a translational unit cell with three spins. (The translational unit cell for the FFTR contains a single spin, although only the paramagnetic state actually has a unit cell with only one spin.) If the sites within the unit cell are labeled counterclockwise from the top as A, B, and C, then the model can be described by saying that the horizontal B—C bonds are modified by multiplying them by the factor η.

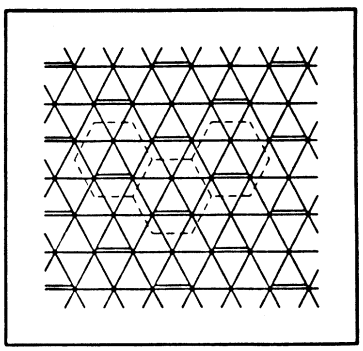

FIG. 1. Bond configuration for the generalized fully frustrated triangular lattice, showing the unit cells. If the lattice sites are labeled counterclockwise from the top as A, B, or C, then the horizontal B—C bonds would be multiplied by the factor η.

Another generalization of the FFTR would be one in which every other row of horizontal bonds becomes $-\eta J$, all other bonds remaining $-J$. This would involve a more complex algebraic analysis, because the unit cell would contain six spins rather than the three of the present case. Moreover, the translational symmetry of the ground state would differ from that of the ground state for the FFTR.

A. Mean-field equations

Including an external field $\mathbf{H}$ along $\hat{\mathbf{y}}$, the XY Hamiltonian is given by

$$\mathcal{H} = -\sum_{\langle ij \rangle} J_{ij}(S_i^x S_j^x + S_i^y S_j^y) - H \sum_i S_i^y , \tag{2.1}$$

with $J_{ij} = -J$ for single bonds, and $J_{ij} = -\eta J$ for double bonds. The brackets in the subscript indicate a sum over nearest neighbors only, with no double counting.

In mean-field theory the effect of finite temperature is to multiply the length of the XY spin by a distribution function $R \leq 1$. In an iterative solution, given a set of spins $\langle \mathbf{S}_i \rangle^{(n)}$ after the nth iteration, the $(n+1)$st set of spins is given by

$$\langle \mathbf{S}_i \rangle^{(n+1)} = \hat{\mathbf{\Phi}}_i^{(n)} R(|\mathbf{\Phi}_i^{(n)}|/T) , \tag{2.2}$$

where the *mean-field* $\mathbf{\Phi}_i^{(n)}$ is given by

$$\mathbf{\Phi}_i^{(n)} = -\left\langle \frac{\partial \mathcal{H}}{\partial \mathbf{S}_i} \right\rangle^{(n)} = \sum_{\langle ij \rangle} J_{ij} \langle \mathbf{S}_j \rangle^{(n)} + \mathbf{H} , \tag{2.3}$$

and T is the temperature ($k_B = 1$). For XY spins the distribution function R is

$$R(x) \equiv I_1(x)/I_0(x) , \tag{2.4}$$

a ratio of modified Bessel functions.[13] In what follows we will consider only converged solutions, and for that reason we will drop the brackets that define the thermal averages.

Thus the mean-field equations for one cell are, in units where $J=1$,

$$\mathbf{\Phi}_1 = \mathbf{H} - 3\mathbf{S}_2 - 3\mathbf{S}_3 , \tag{2.5}$$

$$\mathbf{\Phi}_2 = \mathbf{H} - 3\mathbf{S}_1 - (2+\eta)\mathbf{S}_3 , \tag{2.6}$$

$$\mathbf{\Phi}_3 = \mathbf{H} - 3\mathbf{S}_1 - (2+\eta)\mathbf{S}_2 . \tag{2.7}$$

In Fig. 1 the spins are labeled counterclockwise, with $\mathbf{S}_1$ at the top of each unit cell. For $\eta=1$, Eqs. (2.5)–(2.7) reduce to the FFTR model. Equation (2.6) and (2.7) are symmetrical in the indices 2 and 3, implying that spins $\mathbf{S}_2$ and $\mathbf{S}_3$ will have similar, or correlated, behavior, typically different from $\mathbf{S}_1$.

B. Summary for $\eta = 1$

Reference 7 shows that, in addition to the paramagnetic phase (P), there is a continuously degenerate family of noncollinear, chiral spin states at small H, and a continuously degenerate family of noncollinear, nonchiral spin states at larger H. In the chiral phase an internal rearrangement within a degenerate family of states preserves

the helicity,[14] causing an Ising degeneracy between the positive and negative helicity states. In the nonchiral phase an internal rearrangement will cycle the system through both helicity states. The ground states in a field preserve the $\sqrt{3}\times\sqrt{3}$ periodicity, but the spins are not fixed, satisfying instead the condition $\sum_{i=1}^{3}\mathbf{S}_i=\mathbf{H}/3$, where $|\mathbf{S}_i|=1$ at $T=0$.[5,6] We now present a brief summary, for comparison with our later results.

The chiral-nonchiral transition line can be obtained by requiring $\mathbf{S}_1$ to point along $\hat{\mathbf{y}}$ and the other spins to point opposite to one another along $\pm\hat{\mathbf{x}}$. This leads to the conditions $\Phi_{1y}=H$ and $\Phi_{2y}=H-3S_1=0$, from which

$$H=3R(H/T)\ . \tag{2.8}$$

The $T=0$ intercept is found by setting $R=1$, giving $H_{T=0}=3$. The $H=0$ intercept, or melting temperature, where $H/T\ll 1$, is obtained by setting $R(x)\sim\frac{1}{2}x$, giving $T_{H=0}=1.5$. As remarked above, in zero field the energy scale for the single phase transition that occurs is about a factor of 3 lower in Monte Carlo than in mean-field calculations.[5–7] We would expect the same kind of suppression to occur for $\eta\neq 1$.

The para-nonchiral transition line can be obtained by requiring that the spins in the chiral phase point approach verticality, with $\mathbf{S}_2=\mathbf{S}_3$. This leads to the conditions $\Phi_1=H-6S_2$, $\Phi_2=H-3S_1-3S_2$, and $H=3S_1+6S_2$, from which

$$H=9R(H/3T)\ , \tag{2.9}$$

so that $H_{\text{P-C}}(T)=3H_{\text{C-NC}}(T)$. Equation (2.9) is equivalent to Eq. (20) of Ref. 7. The intersections $H_{T=0}=9$ and $T_{H=0}=1.5$ immediately follow from Eq. (2.9). Since $T_{H=0}=1.5$ for both lines, this is a tricritical point. The mean-field phase diagram is given in Fig. 2 of Ref. 7. Both Ising and XY order set in at the same temperature for $H=0$, a result that also seems to hold in the Monte Carlo case.[5,6,10]

It is important to observe that for $\eta=1$ the sublattices are equivalent, and any permutations of the spins from one sublattice to the other yields a new, degenerate solution. This has relevance for the collinear Potts phase observed in Monte Carlo calculations, where two sublattices order in the same way (along the field), and one sublattice orders differently. *A priori*, there is no way of telling which of the sublattices will order differently from the others, just as there is no way to tell whether an Ising ferromagnet in $H=0$ will order up or down.

III. ITERATION CONTRAST PLOT METHOD

As indicated above, the use of iteration contrast plots permitted us to obtain an overview of the structure of the mean-field phase diagram, before any phases or transition lines had been identified, and prior to solving the mean-field equations analytically. In this method one produces a visual display that indicates the average number of iterations required to reach a specific level of convergence to the solution of the mean-field equations. (Typically, the rms change in the solution, per iteration, was set to be no larger than one part in 10^6, and ten randomly chosen initial sets of spin coordinates were chosen.) For each sampled point in the phase space, a dot is printed whose size is proportional to the average number of iterations multiplied by a nonlinear contrast function (chosen to bring out the most interesting details. Since the number of iterations increases near phase transition lines (because of processes analogous to critical slowing down), these phase transitions usually show up as dark curves against a much lighter background, hence iteration contrast. A two-dimensional (2D) slice of the phase diagram is scanned in two of the variables (T,H,η), while the third is kept fixed; in the present problem, IC plots for constant η were the most useful.

We performed an IC plot analysis for the known case where $\eta=1$, obtaining regions of dark dots in the vicinity of each phase transition. The P region for $H=0$ is always evident in IC plots, probably because there is no mean field to drive the system to a solution. On no occasion did we iterate to solutions that differed from those found analytically by Ref. 7. Given that the mean-field equations are nonlinear, it was by no means guaranteed that the solutions given in Ref. 7 exhausted the possibilities. In particular, the (continuous) internal rearrangement degeneracy, whereby nonsymmetric and very different looking solutions have the same energy, was confirmed by the numerical solutions, even at finite T.

IV. PHASE DIAGRAM FOR $-0.5<\eta<1$

A. General approach

IC plots in (T,H) for constant η, or in (T,η) for constant H, gave a good account of the phase transitions for a given 2D slice through the 3D phase space in T, η, and H. We now turn to the symmetry of each of the phases that appear. For most of this section, we consider the phase diagram in the (T,H) plane for $\eta=0.6$. One can pick any η in the range $-0.5<\eta<1$, since the phase-diagram topology does not change in that range. The chiral phase disappears for $\eta<-0.5$.

B. Phases

We have found four phases, which are given in Fig. 2. The P and Potts-like ferrimagnetic (FI) phases have the same symmetry for $H\neq 0$, where they are related by a continuous transformation. There is an apparent phase transition line for $H\neq 0$, which corresponds to $\mathbf{S}_1=\mathbf{0}$, for which the mean field driving the system to equilibrium is zero, resulting in a slow rate of convergence. Despite this equivalence of P and FI for $H\neq 0$, it will be convenient to consider the paramagnetic phase to have two subphases.

C. Phases FI and C1

In the lower left corner of Fig. 3 is a canted phase, denoted by C1, which is essentially the same as the chiral phase for $\eta=1$. The internal rearrangement degeneracy is no longer present, however, and the spin lengths and angles are different from the analogous $\eta=1$ spin state. In the region labeled "Potts-like," the solution is described by

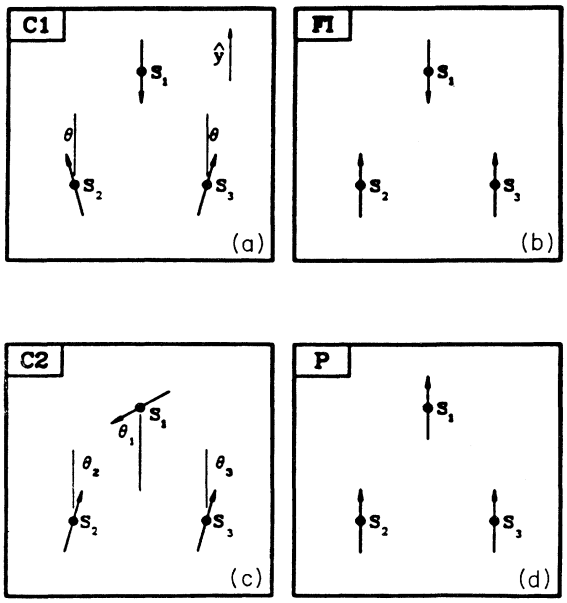

FIG. 2. (a) Particular state in the chiral phase C1 used to get the transition line C1-FI. (b) The spin state in the nonuniform, collinear phase FI. (c) The general form of the state in nonchiral phase C2. See text for detailed explanation. (d) The paramagnetic state P in a field. Note that, for $\eta \neq 1$, $S_1 \neq S_2$, so that P is nonuniform and collinear, as is FI. Indeed, P and FI are the same state, distinguished for our purposes only by the fact that $\mathbf{S}_1$ is along the field in P and against the field in FI.

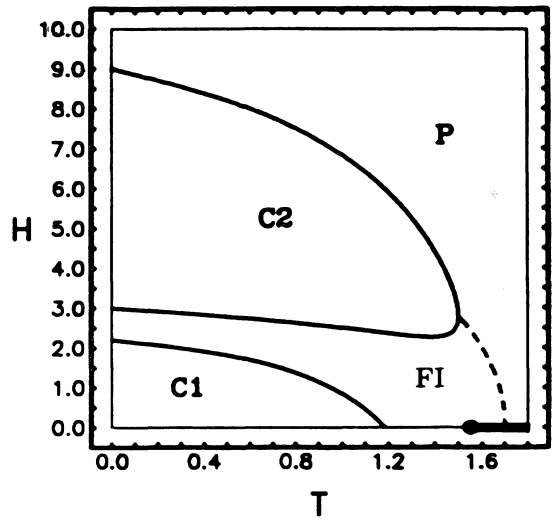

FIG. 3. Phase diagram for the generalized fully frustrated triangular lattice for $\eta = 0.6$. Both axes are given in units of the exchange constant J. Solid lines are phase transition lines. The heavy broken line is the $S_1 = 0$ line separating the P and FI regions of the nonuniform, collinear phase, and the light broken line is the $\eta = 1$ line, added for comparison. Phase names and representative spin states are shown in the four regions separated by the transition lines.

$$\mathbf{S}_1 = -|S_1|\hat{\mathbf{y}}, \quad \mathbf{S}_2 = \mathbf{S}_3 = |S_2|\hat{\mathbf{y}} , \tag{4.1}$$

and is pictured in Fig. 2(b). The C1 state is described by

$$\mathbf{S}_1 = -|S_1|\hat{\mathbf{y}}, \quad S_{2x} = -S_{3x} = S_2 \sin\theta , \quad S_{2y} = S_{3y} = S_2 \cos\theta . \tag{4.2}$$

As can be seen in Fig. 2(a), this phase is similar to FI except that S_2 and S_3 are tipped outward (or inward) by an angle θ.

D. C1-FI line

The C1-FI line is obtained by combining (4.2) with (2.5)–(2.7) in the limit as $\theta \to 0$. This leads to $\Phi_2 = (2+\eta)S_2$. The C1-FI line is then determined by numerical solution of the equations

$$S_2 = R[(2+\eta)S_2/T] , \tag{4.3}$$

$$H + 3R(|H - 6S_2|/T) - 2(2+\eta)S_2 = 0 . \tag{4.4}$$

The $T = 0$ intercept of C1-FI is found from (4.4) by setting $R = 1$ and $S_2 = 1$, giving

$$H_{T=0} = 1 + 2\eta . \tag{4.5}$$

For $\eta \to 1$, $H_{T=0} \to 3$, as expected. Since $H_{T=0} \to 0$ as $\eta \to -0.5$, the phase C1 exists only in the range $-0.5 < \eta < 1$. Note that for $H = 0$ the FI phase truly differs from the P phase. We denote the $H = 0$ P-FI transition temperature by T_I, because the transverse degrees of freedom are expected to produce an Ising transition associated with the twofold degeneracy from interchanging $\mathbf{S}_2$ and $\mathbf{S}_3$. This transition temperature, unlike others for $H = 0$, must be determined numerically.

E. Phase C2

C2 is a canted (noncollinear) phase described by

$$\mathbf{S}_2 = \mathbf{S}_3 . \tag{4.6}$$

There is no continuous degeneracy. As pictured in Fig. 2(c), in C2 spins 2 and 3 tip together at the same small angle θ_2, while spin 1 moves over its entire range $0 \leq \theta_1 < \pi$. Near C2-FI we have $\theta_1 \approx \pi$ [i.e., spin 1 points *down* (against the external field) to match with phase FI], whereas near C2-P we have $\theta_1 \approx 0$ (i.e., spin 1 points *up* to match the P phase). As H increases, spin 1 tips outward one way and spins 2 and 3 tip the other way by a smaller angle, until spin 1 points in the $\hat{\mathbf{x}}$ direction; as H increases further, spin 1 continues tipping toward the $+\hat{\mathbf{y}}$ direction, while spins 2 and 3 *decrease* their tipping.

F. C2-FI and C2-P line

For $H \neq 0$ the phases FI [Fig. 2(b)] and P [Fig. 2(d)] are related by flipping the direction of S_1. We can exploit this to obtain both the C2-FI and C2-P lines by introducing the parameter σ, defined by

$$\sigma = \begin{cases} 1, & \text{spin 1 up, near C2}-\text{P} , \\ -1, & \text{spin 1 down, near C2}-\text{FI} . \end{cases} \tag{4.7}$$

Near the C2-P and C2-FI lines, where the tipping angles θ_1 and θ_2 are small, the mean-field equations (2.5)–(2.7) become, with (4.6),

$$\Phi_1=(-\theta_1,\sigma)\Phi_1=(-6S_2\theta_2,\ H-6S_2)\ , \tag{4.8}$$

$$\Phi_2=(\theta_2,1)\Phi_2$$
$$=(3S_1\theta_1-(2+\eta)S_2\theta_2,\ H-3\sigma S_1-(2+\eta)S_2)\ . \tag{4.9}$$

The ratios of the x and y components of Eqs. (4.8) and (4.9) yield, on elimination of θ_1 and θ_2,

$$H-3\sigma S_1-6S_2=0\ . \tag{4.10}$$

Combined with the Y component of (4.9), (4.10) yields $\Phi_2=(4-\eta)S_2$, and so

$$S_2=R[(4-\eta)S_2/T]\ . \tag{4.11}$$

Equation (4.10) and the y component of (4.8) then yield

$$H-3\sigma R(|H-6S_2|/T)-6S_2=0\ . \tag{4.12}$$

Equation (4.11) and (4.12) are evaluated together to find $H(\sigma T)$ for the C2-FI and C2-P lines.[15,16] It is important to note that, in a field, both the FI and P phases are nonuniform and collinear. Indeed, in a field they have the same symmetry and are the same phase thermodynamically. We distinguish between them because they are distinct in zero field. The phase diagram is given in Fig. 3.

G. Zero-field paramagnetic phase

For $H=0$ and sufficiently high temperatures, the system is in a true paramagnetic phase, with $\mathbf{S}=\mathbf{0}$ on all three sublattices. Below a certain temperature, which we denote by $T_{\rm KT}$, the system goes into a true FI phase. This phase is collinear and has a spontaneous magnetization on each of the sublattices. By analogy with what happens for XY ferromagnets in $H=0$, we expect that this phase is destroyed, not by the local mean-field going to zero, but by a process wherein there is a nonzero local mean field, where vortex-antivortex pairs are thermally generated.[17]

As T approaches $T_{\rm KT}$ from below, the spin lengths $\{S_i\}$ and the mean-field magnitudes $\{\Phi_i\}$ approach zero, and so we can employ $R(x)\approx\frac{1}{2}x$. Thus $\Phi_1\approx 2TS_1$ and $\Phi_2\approx 2TS_2$, where $\Phi_1=-6S_2$, $\Phi_1=3S_1-(2+\eta)S_2$, from which we find

$$T_{\rm KT}(\eta)=\tfrac{1}{4}\{[(2+\eta)^2+72]^{1/2}-(2+\eta)\}\ . \tag{4.13}$$

$T_{\rm KT}$ $(\eta=1)=1.5$, as expected, $T_{\rm KT}$ $(\eta=-0.5)=1.7792$ when the C2 phase disappears, and $T_{\rm KT}$ $(\eta=0.6)=1.5687$. The latter value is in good agreement with Fig. 4, where the true P phase can be seen as a dark line of "big dots" along $H=0$ starting very near $T=1.59$ and continuing out to larger T.[18]

H. FI-P transition line

This line only occurs for $\eta<1$, where it is possible to have collinear phase for which $\langle\mathbf{S}_1\rangle=\mathbf{0}$ and

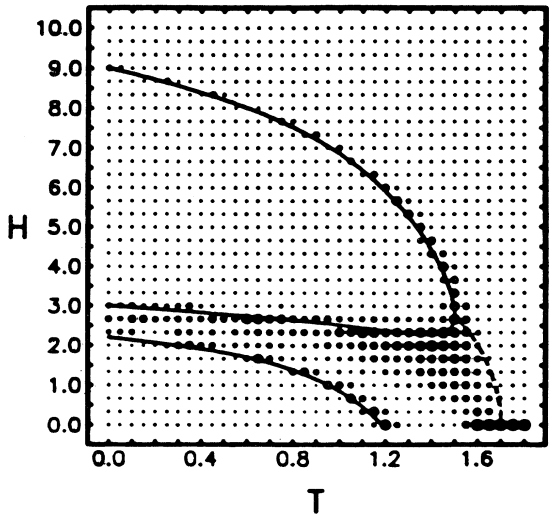

FIG. 4. $\eta=0.6$ transition lines from Fig. 3 overlaid on the $\eta=1$ IC plot. Both axes are given in units of the exchange constant J. The two match well except for the $S_1=0$ line in the lower right: Here the IC plot is blurred, but for $H=0$, the intersection point of the analytic line agrees with the start of the zero-field P phase (dark line of dots).

$\langle\mathbf{S}_2\rangle=\langle\mathbf{S}_3\rangle\neq\mathbf{0}$. This occurs when $\Phi_1=H-6\langle S_2\rangle=0$ and $\Phi_2=H-(2+\eta)\langle S_2\rangle$, which combine to yield

$$H-6R[H(4-\eta)/6T]=0\ . \tag{4.14}$$

The $H=0$ intercept is found by applying $R(x)\to x/2$ as $x\to 0$ to (4.14), which gives

$$T_{H=0}=2-\tfrac{1}{2}\eta\ . \tag{4.15}$$

For $\eta=1$ this is in agreement with earlier results, and for $\eta=0.6$ we get $T_{H=0}=1.7$, in agreement with Fig. 3.

The FI-P line has two end points, one given by (4.15) and the other by its intersection with the C2 phase, which occurs where the C2-FI and C2-P lines meet. This specifies a point (H_A,T_A) whose coordinates, in principle, depend on η. From (4.10), as $S_1\to 0$, we obtain $H-6S_2\to 0$. Then the evaluation of (4.12) in this limit yields

$$T_A=1.5\ , \tag{4.16}$$

independent of η. Using this value of temperature in (4.11), (4.10) becomes, for $S_1\to 0$,

$$H_A-6R[H_A(4-\eta)/9]=0\ . \tag{4.17}$$

This gives H_A $(\eta=1)=0$, as expected, and for $\eta=0.6$, H_A is in good agreement with the value found in Fig. 3. Note that H_A increases very quickly as η decreases from 1. Also, as $\eta\to-\infty$, $H_A\to 6$.

V. PHASE DIAGRAM FOR $\eta > 1$

A. Phases

The IC plot indicated that there are four phases, the state P given in Fig. 2, and three others, given in Fig. 5. However, C3 and C4 are clearly equivalent to one another and are used to distinguish between the cases $S_{2y} > 0$ and $S_{2y} < 0$. The phase diagram is given in Fig. 6.

The spin state in the lower region of Fig. 6, denoted by C3, is pictured in Fig. 5(a) and is described by

$$\mathbf{S}_1 = S_1 \hat{\mathbf{y}}, \quad S_{2x} = -S_{3x} , \tag{5.1}$$

where $S_{2y} = S_{3y} < 0$. The upper region, denoted by C4, is pictured in Fig. 5(b) and is the same as C3 except that $S_{2y}, S_{3y} > 0$. The C3-C4 line is characterized by (5.1) and

$$S_{2y} = -S_{3y} . \tag{5.2}$$

Actually, spins 2 and 3 are free to rotate around the positions shown in Fig. 5(c), since they make a null contribution to the Hamiltonian (2.1). Thus this line is characterized by a degeneracy in the solution. To the right of the large dot mentioned above is a true antiferromagnetic (AF) phase, located between the dot and the P transition, on the $H = 0$ line. As can be seen in Fig. 5(d), spin 1 here is "melted," i.e., $S_1 \to 0$. The P phase is shown in Fig. 2(d).

Note that in the IC plot (not shown) there was a light band corresponding to the C3-C4 line, which is probably due to the degeneracy described above (the attractor is a circle instead of a point). The adjacent regions were dark, probably because of a shallow minimum associated with a solution that is unique (except for interchange of S_2 and S_3), with S_2 and S_3 pointing almost normal to the field.

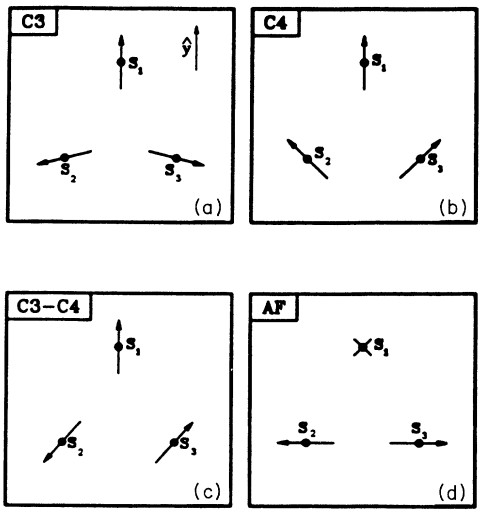

FIG. 5. (a) $\eta > 1$ spin state in phase C3. (b) The spin state phase C4. (c) A particular spin state of the C3-C4 line, the degenerate "dividing" phase between the C3 and C4 regions. Spin 1 is fixed as shown, but spins 2 and 3 can rotate, obeying the condition $\mathbf{S}_2 = -\mathbf{S}_3$. (d) The $H = 0$, pure AF phase. The $\times$ at position 1 means that spin 1 is melted, i.e., $S_1 = 0$.

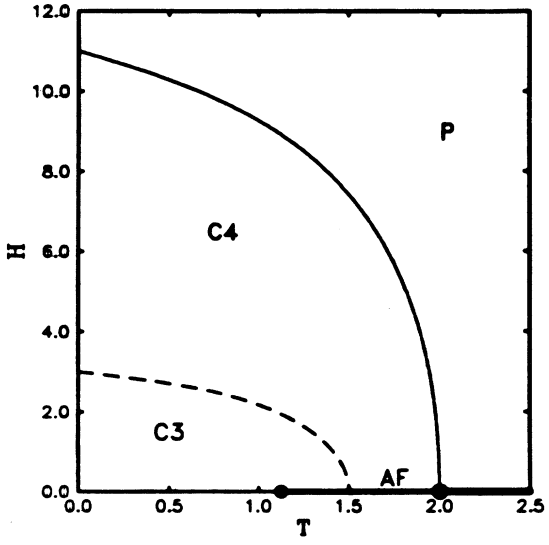

FIG. 6. Mean-field phase diagram for $\eta = 2$. Both axes are given in units of the exchange constant J.

B. C3-C4 (inner) line

Conditions (5.1) and (5.2) lead to Eq. (2.8), so that the C3-C4 line for $\eta > 1$ is the same as the C1-C2 line for $\eta = 0$. In particular, the $T = 0$ and $H = 0$ intersections are, as before, at $H = 3$ and $T = 1.5$.

C. C4-P (outer) line

The equations yielding this line are (4.3), as in the $\eta < 1$ case, and

$$H - 3R\,(|H - 6S_2|/T) - 2(2+\eta)S_2 = 0 , \tag{5.3}$$

which is similar to Eq. (4.4). The $T = 0$ intercept of the C4-P line is $H_{T=0} = 7 + 2\eta$. The $H = 0$ intercept is determined from $S_1 = 0$, $S_2 \to 0$, which from (4.3) yields

$$T_{\mathrm{KT}}(\eta > 1) = 1 + \tfrac{1}{2}\eta , \tag{5.4}$$

where we use the notation T_{KT} for the reason discussed in the previous section. As η increases, the entire C4-P line moves outward, in contrast to the C2-P line of $\eta < 1$, which is fixed at the top near $T \approx 0$ and undergoes qualitative changes for higher T.

D. AF phase

This state occurs along the $H = 0$ line and is pictured in Fig. 5(d): Spin 1 is "melted," while spins 2 and 3 oppose each other. The IC plot of Fig. 4 indicates that it occurs for $H = 0$, $T_{\mathrm{AF}} < T < T_{\mathrm{P}}$. The $H = 0$ mean-field equations for the temperature at which S_1 first differs from zero, so that S_2 and S_3 tip together, lead to $\Phi_{1y} \approx -6S_2\theta_2 \approx 2TS_1$, $\Phi_{2x} \approx \theta_2\Phi_2 \approx -3S_1 - (2+\eta)S_2\theta_2$,

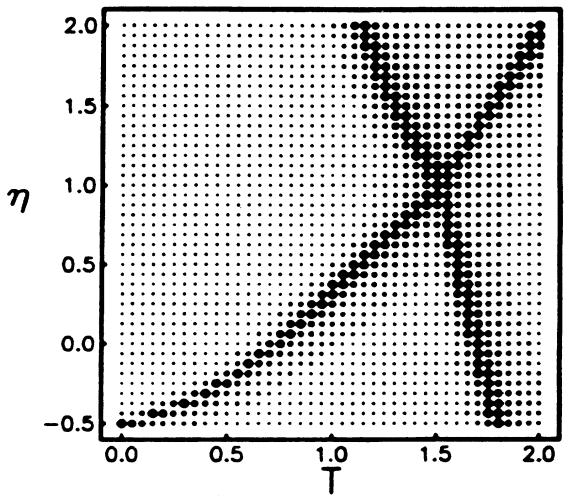

FIG. 7. IC plot for the $H=0$ plane. Both axes are given in units of the exchange constant J.

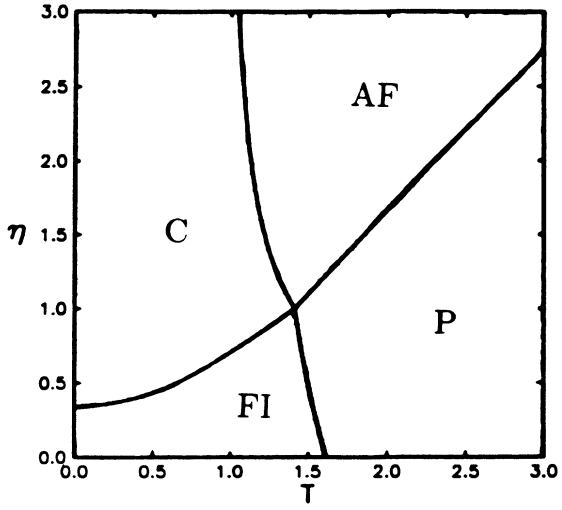

FIG. 9. Mean-field phase diagram for $H=0$ in the generalized Villain model, from Gabay *et al.* (Ref. 9). Both axes are given in units of the exchange constant J.

and $\Phi_2 \approx (2+\eta)S_2$, which lead to

$$T_I(\eta>1)=\frac{9}{2(2+\eta)} \ . \tag{5.5}$$

Figure 6 gives the mean-field phase diagram for $\eta=2$.

VI. ZERO-FIELD PHASE DIAGRAM

In addition to the planes of constant η, we can consider phase diagrams in planes other than (T,H). For example, a section $(0\le T\le 2,\ -0.5\le\eta\le 2)$ of the $H=0$ IC plot is shown in Fig. 7. There are four regions, separated by either a dark band or an edge. On the far right, at large T and small η, is the P phase.[18] The triangular region at the bottom, for $\eta<1$, is the true FI phase, whose boundary with the P phase is described by Eq. (4.13). The triangular region at the top, for $\eta>1$, is the true AF phase, whose boundary with the P phase is given by $T_{\rm KT}=1+\frac{1}{2}\eta$. The left upper triangular region consists of the C1 $(\eta<1)$ and C3 $(\eta>1)$ phases, both of which are noncollinear. The $\eta=1$ line does not appear in the IC plot because the $\eta=1$ internal rearrangement degeneracy, by increasing the available phase space of convergence points, decreases the number of iterations required, effectively canceling any phase-transition-induced dark band. Moreover, the C1 and C3 phases should not be considered to be distinct, since they have the same symmetry, going continuously into one another for $\eta=1$ because of the $\eta=1$ internal rearrangement degeneracy. There is a single multicritical point, given by $T=1.5$ and $\eta=1$. Figure 8 gives the full $H=0$ phase diagram, with representative spin states in each phase.

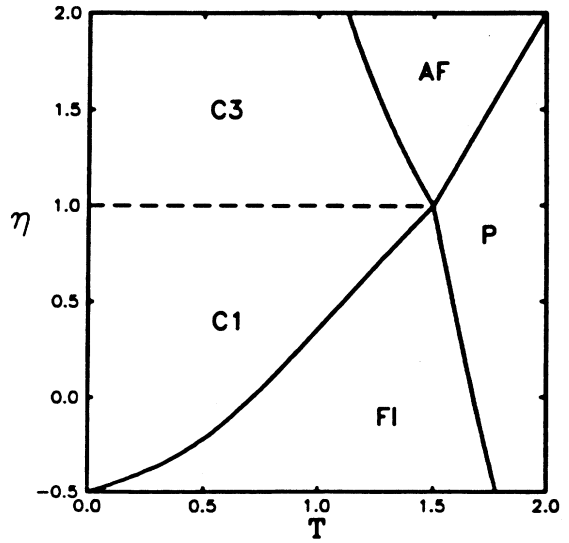

FIG. 8. Mean-field phase diagram for the $H=0$. Both axes are given in units of the exchange constant J. The C1 and C3 phases should not be considered to be distinct.

We now compare the $H=0$ mean-field phase diagrams of the generalized FFTR model and the generalized Villain model.[8] (Berge *et al.* introduced tunable frustration and investigated the Monte Carlo phase diagram for $H=0$ in order to determine whether the $\eta=1$ transition was of an Ising or Kosterlitz-Thouless character.) The latter is shown in Fig. 9. Figures 8 and 9 show a general topological similarity, although the actual phase boundaries are described by different equations. In Fig. 9 the phases P, FI, AF, and C correspond to, respectively, phases P, FI, AF, and C1–C3 in Fig. 8.

VII. SUMMARY AND CONCLUSIONS

We have generalized the fully frustrated triangular lattice of XY spins, so that the system need not be fully frustrated. In zero field, the mean-field phase diagram is very similar to that of the generalized fully frustrated square lattice of XY spins,[8] where the Ising and Kosterlitz-

Thouless transitions occur at the same temperature when the system is fully frustrated, and $T_I < T_{KT}$ otherwise. In a field, and for the parameter $\eta < 1$, the mean-field phase diagram for the present model bears a superficial similarity to that of the Monte Carlo phase diagram for $\eta = 1$, but no true Potts phase appears, since the sites are not equivalent; unlike what happens for the $\eta = 1$ Monte Carlo phase diagram, where a discrete symmetry of the Hamiltonian is spontaneously broken, the "different" sublattice is built into the Hamiltonian when $\eta \neq 1$.

In retrospect, finding the Potts phase in Monte Carlo calculations for XY spins in the FFTR should not be surprising; the Potts phase had already been found in Monte Carlo calculations by Metcalf for Ising spins in the FFTR.[19] The difference between the Ising and XY cases is that on going from the Ising case (where only the Potts and the paramagnetic phases were present) to the XY case, one finds that the chiral C1 phase makes an incursion into the Potts phase at low fields and low temperatures, and the nonchiral C2 phase makes an incursion into the Potts phase at higher fields and low temperatures.

From the point of view of energy scales, when there is an applied field the longitudinal spin components may be thought of as having a higher-energy scale than the transverse spin components. Once the Potts phase interposes itself at low T for H/J near 3, the transverse fields become less effective, and the system has a greater tendency to become collinear. This is similar to what happens in a model we have proposed to explain reentrance in spin glasses, where the "frustrated" spins "melt" at a lower temperature than the "host" spins, thereby enabling the system to become collinear at an elevated temperature.[20] Note that a real-space renormalization-group analysis for the Ising spin case has been performed[21] and is in good agreement with Metcalf's Monte Carlo studies.[19]

Another insight into the origin of the Potts phase in the FFTR comes from the work of Kawamura, who considered the problem of the phase diagram for this system by including in the free energy the entropy of the thermal fluctuations about the equilibrium state.[22] In this analysis (which is restricted to low temperatures), the spins themselves are visualized and in different field regimes are found to be the same as the C1, C2, Potts, and p phases, in agreement with a symmetry analysis of the Monte Carlo calculations. Moreover, for $H = 3$, although in mean-field theory the C1, C2, and Potts solutions are degenerate and can be connected continuously by the sliding degeneracy found by Ref. 7, Kawamura's analysis shows the Potts phase to be favored, again as found in the Monte Carlo calculations.

We close by remarking that the energy scale argument given above also serves to explain why, in zero field, XY spins on fully frustrated lattices have both Ising and Kosterlitz-Thouless transitions occurring at the same temperature. Namely, both longitudinal and transverse energy scales are the same. Thus, if longitudinal order exists locally, so does transverse order (and vice versa), and hence helicity can be defined. As a consequence, both the continuous orientational order and the discrete helicity order coexist, and the loss of either implies the loss of the other. For $\eta \neq 1$, however, this longitudinal-transverse degeneracy is broken. As a consequence, when the temperature is raised, the low-temperature state where both longitudinal and transverse order occur (for which there is both continuous orientational order and discrete helical order) goes into a state where only longitudinal or transverse order occurs (for which there is only continuous orientational order). The loss of the discrete helicity order corresponds to an Ising transition. At a higher temperature the orientational order is also lost because of the generation of topological excitations (the Kosterlitz-Thouless mechanism[17]).

---

[1]For an excellent review of spin glasses, see K. Binder and A. P. Young, Rev. Mod. Phys. **58**, 801 (1986).

[2]J. Villain, J. Phys. C **10**, 1717 (1977).

[3]H. T. Diep, A. Ghazali, and P. Lallemand, J. Phys. C **18**, 5881 (1985).

[4]G. Wannier, Phys. Rev. **79**, 357 (1950); Phys. Rev. B **27**, 5017 (1973).

[5]D. H. Lee, J. D. Joannopoulos, J. W. Negele, and D. P. Landau, Phys. Rev. Lett. **52**, 433 (1984).

[6]D. H. Lee, J. D. Joannopoulos, J. W. Negele, and D. P. Landau, Phys. Rev. B **33**, 450 (1986).

[7]D. H. Lee, R. G. Caflisch, J. D. Joannopoulos, and F. Y. Wu, Phys. Rev. B **29**, 2680 (1984).

[8]B. Berge, H. T. Diep, A. Ghazali, and P. Lallemand, Phys. Rev. B **34**, 3177 (1986).

[9]M. Gabay, T. Garel, G. Parker, and W. M. Saslow, Phys. Rev. B **40**, 264 (1989).

[10]S. Miyashita and H. Shiba, J. Phys. Soc. Jpn. **53**, 1145 (1984). This work, employing a 36-state clock model, found T_I slightly larger than T_{KT}, a result that may be explained if the statistical uncertainty were larger than originally estimated.

[11]For a recent review, see Physica B **152**, 1 (1988).

[12]For recent work in this direction, see H. Eikmans, J. E. Hinbergen, H. J. F. Knops, and J. M. Thijssen, Phys. Rev. B **39**, 11 759 (1989).

[13]For comparison, $R(x) = \tanh(x)$ for Ising spins and $R(x) = 1/\tanh(x) - 1/x$ for Heisenberg (3D) spins.

[14]The helicity can take three values only, $\pm 1, 0$, and is defined as $\sum_i \Delta\theta_i / 2\pi$, where $\Delta\theta_i$ is the smallest change in angle when each triangle is traversed in a clockwise fashion. An alternate definition is $(2/3\sqrt{3})(\mathbf{S}_1 \times \mathbf{S}_2 + \mathbf{S}_2 \times \mathbf{S}_3 + \mathbf{S}_3 \times \mathbf{S}_1) \cdot \hat{\mathbf{z}}$, where 1, 2, and 3 are vertices of a triangle transversed in a clockwise fashion.

[15]We used the method of bisection to numerically evaluate formulae involving the function $R(X)$.

[16]Note that the step size ΔT must be decreased as $T \rightarrow 1.5$, when solving for $H(T)$ numerically.

[17]J. M. Kosterlitz and D. Thouless, J. Phys. C **5**, 124 (1972); **6**, 1181 (1974); J. M. Kosterlitz, *ibid.* **7**, 1046 (1974).

[18]In an IC plot any part of an $H = 0$ paramagnetic region shows

up as a solid line or a solid block of dots.
[19]B. D. Metcalf, Phys. Lett. **45A**, 1 (1973).
[20]W. M. Saslow and G. N. Parker, Phys. Rev. Lett. **56**, 1074 (1986).
[21]M. Schick, J. S. Walker, and M. Wortis, Phys. Rev. B **16**, 2205 (1977).
[22]H. Kawamura, J. Phys. Soc. Jpn. **53**, 2452 (1984).